



university of
groningen

faculty of mathematics
and natural sciences

———— Physics of Quantum Devices ——

Excited State Spectroscopy and Optical Bleaching in c-axis divacancies in Silicon Carbide

December 12, 2015

By:

Joop Age Harm Adema
S2406942

Supervised by:
van der Wal, C.H.
Zwier, O.V.
Palasantzas, G.

Abstract

C-axis divacancy bound electron spins in Silicon Carbide (SiC) have interesting properties for quantum information applications. SiC is a material well known to large scale industrial processing and spin states in the ground state of the divacancy show coherence times (T_2^*) up to the millisecond scale.

This thesis addresses two main issues regarding optical manipulation ensembles of c-axis divacancies in SiC: the process of charge state switching (optical bleaching and repumping) and the yet unknown excited state structure of c-axis divacancies.

Using several rates of illumination, optical bleaching processes were analyzed by fitting bleaching traces to an exponential decay, with a decay constant depending on transition linewidth, laser field spatial distribution and the power of laser intensity. The model along which the bleaching process was fitted was not able to make a perfect fit attributed to other absorption processes, especially not for higher laser intensities. By considering the best fit of the model to the bleaching traces and the shape of the bleaching curves for different powers of the intensity, it was found that a single photon process is probably underlying the bleaching process. Possible excitations that could cause bleaching effect have been proposed and suggestions for improvement of the method to investigate which processes cause both charge state switching effects have been posed. The repump process was not considered thoroughly due to absence of a continuous wave laser in the range of optical wavelengths able to restore the divacancies in the resonant charge state.

Magneto-spectroscopy was performed to evaluate the excited state structure by considering electronic levels and transitions and their respective spin pumping features. Using a lock-in technique in transmission, the persistent absorption by electrons which underlined spin pump features was probed by magneto-spectroscopy. These features did not correspond to features expected as the result of a triplet-triplet electronic structure, but belonged to two different sets of carrier frequencies. To explain this behavior, three possible hypotheses are posed: a manifold excited state with differing transition strengths and Inter System Crossing (ISC) strengths, two different physical defects with both a triplet excited state with differing transition and ISC strengths and a single defect where local strain discontinuously alters the transition and ISC strengths and electronic structure. Moreover, several suggestions for testing these hypotheses are given.

Bachelor's Thesis

**Public Presentation: 08-12-2015
5113.0201, 15:00, University of Groningen**

Contents

1	Introduction	2
1.1	C-axis defects in Silicon Carbide	2
1.2	This thesis	2
2	Theory	4
2.1	Coherent Population Trapping	4
2.2	Spin state coherence	4
2.3	Other materials and spin manipulation	4
2.4	Electronic levels and transitions in SiC divacancies	5
2.5	Spin pumping features	5
2.6	Optical bleaching	7
3	Exploring the Excited State Structure by Magneto-spectroscopy	8
3.1	Spin pumping features by magneto-spectroscopy	8
3.2	Spin pumping features in a simple triplet-triplet model	10
3.2.1	Triplet-triplet model	10
3.2.2	Fit of magneto-spectroscopic features to model	11
3.3	Excited state structure	13
3.3.1	Independence of two sets of spin pumping features	13
3.3.2	Excited state structure hypotheses	14
3.4	Asymmetric CPT in c-axis defects	14
4	Optical Bleaching in C-axis Divacancies	16
4.1	Temporal bleaching traces	16
4.2	Bleaching model	17
4.3	Results	18
4.3.1	Fit of traces to model	18
4.3.2	Fit of bleaching shapes to traces	19
5	Conclusion	23
5.1	Excited state structure	23
5.2	Optical bleaching	23
5.3	Conclusion	24
	References	25
A	Frequency Spectra of IDQ ID230 Photon Counter Signal	26
B	Hamiltonian of a Triplet Orbital State	26

1 Introduction

In recent years, many developments in the field of quantum information physics and more specific the characterization of potential quantum bit (qubit) systems have gained significant interest. Part of this research consists of methods that optically address ensembles of atoms or lattice defects. Next to research about writing, storing and reading out quantum states, research efforts are directed towards the more practical side of designing systems which can compute and communicate with other systems using quantum bits as well.¹

For particular quantum cryptography schemes, it is impossible to copy quantum state information without changing the information itself. Hence, eavesdropping can be noticed and the information flow can be stopped, such as with a quantum cryptography protocol based on entanglement between the sender and receiver key.² The implications of this protocol are similar to the BB84 encryption protocol, which uses the public discussion of a pair of randomized keys *after the signal has been sent*. Intercepting and resending correctly can only be performed in a BB84 encryption if one guesses the randomized key of the sender exactly. When resending includes mistakes by not knowing the sender key, errors will be detected during the public discussion of keys; the procedure can be immediately aborted. However, a single public discussion can not be of such size or such format that it includes useful information on its own, since eavesdropping has taken place before the process could be aborted.³

Moreover, the classical limit for memory storage density and computational density is nearby, since classical electronics have become of the size where they face distortive quantum tunneling effects. A compelling measure of computation density is the size of transistors, which has dramatically decreased in the past 30 years.

An electronic qubit uses the superposition between - for example - both electron eigenstates to form a quantum state:

$$|\psi\rangle = \alpha|\uparrow\rangle + \beta|\downarrow\rangle$$

With such a superposition of two states, with which one could build a computational network. Quantum networks can store more information than classical networks of classical bits can. A network with k nodes of n individual qubits has a space of 2^{kn} dimensions, whereas a classical system only had 2^n dimensions.¹ Hence, if it is possible to address dense single or a few-atom qubit systems, the classical limit for information storage and computing power density can be trespassed.

Both quantum cryptography able to prevent eavesdropping and the prospect of improved information storage and computing power density make qubit based information systems desirable for computation and communication networks. Although qubit systems still have to undergo the development from a proof of principle to a fully operational system of data processing and network protocols for data transport, many research efforts in various materials and various spin manipulation schemes have been and are being performed.¹

1.1 C-axis defects in Silicon Carbide

The divacancy (V_{SiC}) colour centre in Silicon Carbide (SiC) has desirable properties to be a qubit candidate. The divacancy is a deep-lying defect, which means that the electronic structure is far within the band gap of the surrounding material (see figure 1.1). Besides, the spin states of the divacancy are long living, meaning that the relaxation of higher to lower ground states is a rather slow process. The divacancy consists of adjacently a missing silicon and carbon atom in the lattice of SiC. SiC is an industrially processed material and it is possible to increase the amount of divacancies in the material by striking the material by electrons accelerated to energies of several MeV. A broad variety in SiC crystal structure exists, which is due to its different hexagonal packing structures. In this thesis, the PL2 crystal growth axis (c-axis) divacancies of 4H-SiC with a band gap of 3.23 eV are optically manipulated.^{4,5} 4H-SiC is stacked in a hexagonal ABCB-configuration, where the '4' refers to the stacking periodicity. Next to the c-axis divacancies, divacancies can also be directed in the basal plane direction. However, the basal plane has more non-degenerate variants than the c-axis, which makes the c-axis a more compelling candidate for coherent spin manipulation. The ground states of divacancies in SiC are pure triplet ($S = 1$) states for finite magnetic field values. The ground state splitting between the $m_s = 0$ level and the average of $m_s = 1$ and $m_s = -1$ energy levels is given by $D_g = 1.305$ GHz and for the energy difference between the $m_s = -1$ and level $m_s = 1$ is $E_g \approx 0$ GHz, all at 0 magnetic field.⁶ The dominant transition frequency, the Zero Phonon Line (ZPL), of c-axis divacancies is in the infrared range: it occurs at 1130.6 nm.⁵

1.2 This thesis

In this thesis, I will discuss research performed on optical bleaching in PL2 c-axis divacancies in SiC. Besides the excited state structure of these divacancies has been studied. Both subjects are essential to understand the

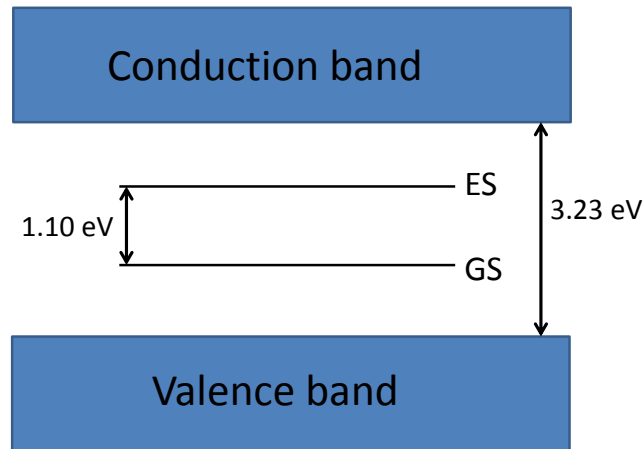


Figure 1.1: *The simplified energy band structure of the divacancy in SiC with a single ground and excited state. The band gap of SiC and ZPL energy of the PL2 divacancy are shown by double arrows.*

entire electronic structure and physical processes governing electron behavior in divacancies in SiC, which is essential for designing reliable quantum bit systems.

Chapter [2] and [3] discuss the underlying theory and methods used to investigate the concerns of chapters [4] and [5]. By magneto-spectroscopic methods (see section [3.2]), the electronic structure of the divacancies is probed and compared to a model assuming a simple triplet excited state structure. Moreover, chapter [4] poses several excited state hypotheses for explaining the magneto-spectroscopic features observed. The effect of optical bleaching is investigated by fitting temporal traces of the bleaching effect for different illumination intensities and fitted to a functional form in chapter [5]. Chapter [6] gives conclusions of the previous chapters, recommendations for improvement of experimental methods to better understand the processes discussed in chapters [4] and [5] and a general outlook concerning the use of divacancies for quantum bit applications.

2 Theory

This chapter gives an overview of methods by which electron spins can be polarized in a quantum state in V_{SiC} ([2.1]), the limitations of that ([2.2]) and other materials and methods used for electron spin manipulation ([2.3]). Besides, the last three sections show the essential processes for understanding electronic levels and transitions in divacancies ([2.4]) and the splitting of electronic levels giving rise to spin pump schemes ([2.5]) and the process of optical bleaching ([2.6]).

2.1 Coherent Population Trapping

A mechanism by which electron spins within an ensemble of SiC divacancies can be polarized in a controllable spin state is Coherent Population Trapping (CPT). CPT arises when two laser fields coupling to two ground states are close to resonance with transitions to a single excited state. This so-called Λ -configuration, further discussed in section [2.6], shows destructive interference if both lasers are close to resonance.^{7,8} Due to this interference, the effective excited state population will be negligibly small and the range of two-laser frequency difference (referred to as detuning) where CPT occurs is rather small.⁷ By adjusting Rabi frequencies, one can prepare a certain quantum state in the well-known triplet ground state.⁶

The Hamiltonian belonging to the perturbation of the defect's Hamiltonian in the rotating wave approximation by applying laser fields of a three level electronic structure is given in Appendix [B].^{8,9} Diagonalization of the Hamiltonian gives the dressed states due to the applied laser field. One of the dressed states is a 'dark state', given by:⁷

$$|\Psi\rangle = \Omega_p|g_l\rangle - \Omega_c|g_m\rangle + 0|g_u\rangle \quad (1)$$

Here, g_l, g_m, g_u denote the lower, middle and upper ground state, respectively. Hence, the excited state electron population is zero and there won't be any absorption of photons by divacancy bound electrons in the ideal CPT case. Ω_p and Ω_c are the relative Rabi frequencies of the coupling and probe laser (see section [3.1]). Therefore, one can control the electron population and thus the spin state of the system in steady state. However, the relative CPT signal is limited by inhomogeneous broadening of energy levels (see section [2.4]) and hence transitions, since it only occurs in a small subset of defects closely resonant to the laser fields applied. Therefore, if the inhomogeneous broadening is severe, the decrease in absorption due to CPT will not be large. However, dephasing and spontaneous emission (in the case of some excited state population) limit the coherence time of the initialized spin state once illumination is aborted. To arrive at a solution for the obtained state including these effects, the master equation in Lindblad form of atomic density needs to be solved, as given in literature.¹⁰

2.2 Spin state coherence

Although divacancies in SiC and other defects in different materials (see section [2.3]) are promising quantum bit candidates, a practical problem is the limited practical spin coherence time, T_2^* . The fundamental limit of the coherence time for a given electron spin is T_1 , which is the characteristic time it takes before all electron spins decay to the lowest energy level, possessing a different spin projection. T_2 is the time it takes for a two-state dephasing effect to disturb the quantum phase of the electron spin. T_2^* differs from T_2 , since T_2^* is the decoherence time for an entire ensemble of spins that is manipulated. The dephasing processes limiting spin storage times are mainly due to its solid state environment, such as interaction with fluctuating nuclear spins.⁶ For Electron Paramagnetic Resonance (EPR) schemes, T_2 coherence times have been measured up to hundreds of microseconds by Ramsey decay measurements.⁵ For CPT-schemes, T_2^* coherence times are found to be much lower, attributed to a fluctuating Stark effect inherent to strong laser intensities, continuous illumination and strong strain sensitivity.^{7,11} By means of Dynamic Nuclear Polarization (DNP), it has been shown that the nuclear spins of the Si-29 isotopes in SiC can be polarized almost completely.⁶ Optically pumped electron spin polarization is transferred to the nuclear spin bath by tuning the electronic levels to anticrossings by Zeeman splitting. Nuclear polarization can enhance coherence times, since fluctuations of nuclear spin reduce electron spin coherence.

2.3 Other materials and spin manipulation

This section gives a brief overview of the different materials and schemes that have been used for quantum state manipulation that are most worth mentioning.

Two distinct types of spin manipulation can be performed. One can optically address an ensemble of many defect bound electron spins (or other configurations that resemble similar effects) or a single defect bound

electron spin. Single spin communication requires more precise alignment and foremost detection, but is more robust to broadening due to multiple defects having different strain and crystal-field splittings.¹² Therefore, the coherence time of a single defect (T_2) is larger than that of an ensemble of defects (T_2^*).

Not only divacancies in SiC have been studied for such spin manipulations, but also the very similar NV-center in diamond and rare earth composites. The NV-center in diamond has a very alike geometry as the c-axis divacancy in SiC, since both deep-lying defects show a $C3v$ -symmetry.¹³ Therefore, this thesis uses the better known NV-center as a reference for optical bleaching and excited state structure in SiC divacancies. CPT has also been shown in the negative charge state in NV-centers.¹⁴

Coherence times have been increased in rare earth materials (which are characterized by narrow linewidths) using sophisticated spin echo techniques.¹⁵ However, rare earth materials do not have the favorable properties that are common to currently used solid state materials such as diamond and silicon carbide, such as large natural abundance and knowledge through current use for device processing. In rare earth materials, very long storage times using CPT schemes and dynamic decoupling to reduce hyperfine fluctuations have been shown.¹⁶ Group velocities as low as 45 ms^{-1} have been reported using auxiliary laser fields to excite a third excited state not involving in CPT.¹⁷ Pulse storage has been proven possible when control pulse intensity is reduced to zero and readout is possible by restoring the control pulse.

2.4 Electronic levels and transitions in SiC divacancies

The Photoluminescence (PL) emission spectrum of excited electrons in PL2 divacancies in SiC is characterised by a Zero-Phonon Line (ZPL) at 1130.6 nm and a sideband of phonon-assisted transitions.⁷ The ZPL and phonon-assisted sideband are the frequency dependent characteristics of the absorption and emission spectrum of a particular electronic transition. The intensity of the zero phonon line is generally much higher than that of the phonon side band. The exact emission spectrum can be investigated by PL measurements.⁵

Electronic transitions are the result of the level structure of an electronic configuration. These transitions are not of one particular frequency, but the levels have a particular linewidth, subject to broadening under several circumstances, so the transition frequencies have a particular range of resonance as well.

Two different types of broadening of electronic levels can be distinguished. Broader level widths give rise to broader transition widths, which increases the range of photon frequencies absorbed by the transition. Homogeneous broadening is broadening that is identical for all similar divacancies: an example of this is the broadening of transitions upon heating. The width of the ZPL has been found to be dependent on T^7 in the similar NV-centers.¹⁸

Inhomogeneous broadening is not identical for all defects and depends on the local environment of the divacancy: spatially inhomogeneous hyperfine splitting due to the nearest nuclear spins and Stark splitting due to spin-spin interactions induced by lattice strain are examples hereof.

The width of transitions of c-axis divacancies is around 100 MHz and the inhomogeneous broadening due to crystal field Stark effect by lattice strain is around 50 GHz for one specific sample of SiC. Since this broadening is expected to be bigger (and confirmed in section [5]) than the energy level splitting between excited state levels, a given laser field can be resonant with a certain transition within a specific divacancy and with another transition within another inhomogeneously broadened divacancy. Due to this, coherent control is limited, since one can not address a particular transition solely.

2.5 Spin pumping features

For the case of a triplet ground state with a manifold excited state, as expected from the similarities to NV-centers, a few conditions must be met to detect a signal by two-laser magneto-spectroscopy (as explained in section [3.2]). Both a magnetic field must be present and electron population should not pile up in a non-resonant ground state.

By applying a magnetic field, the electronic transitions within the divacancies are dipole allowed and the levels are splitting dependent on their spin projection, which governs the available transitions. One is able to detect a signal if light is continuously emitted by pathways that are resonant with laser fields pumping ground state electrons back to excited state levels where they can emit a photon again. Methods for collecting this signal is given in section [3.2]. Due to the electrons continuously pumped back and forth to electronic levels resembling different electron spin projections, these features observed in magneto-spectroscopy are called spin pump features.

If all transitions to a particular ground state are allowed, that ground state should be excited by a laser to prevent the electrons to pile up in that level. Similarly, if no transitions are forbidden at all, all ground states should have a transition resonant to a present laser field in order to show spin pumping. Using this criterion for spin pump features, excluding (nearly) forbidden transitions and Inter System Crossing (ISC), we can

distinguish two types within the family of spin pump schemes for a two-laser experiment for two triplet states. Electronic transitions their probability depends on the transition dipole moment of the wavefunctions of the respective levels; hence transitions can be very weak or even forbidden. By ISC it is able for an electron to relax from the excited state to the triplet ground state without emitting a photon. The electron ‘crosses’ from a triplet excited state to a singlet state back to the ground state. For a triplet excited state, the types of spin pumping schemes are shown in figure 2.1. The condition of two transitions being of equal frequency is necessary to show spin pumping features for a two laser experiment, which is graphically denoted by horizontal bars on the transition arrows in figure 2.1. However, if ISC and differing transition strengths are present, the conditions for spin pumping features to occur, change accordingly.

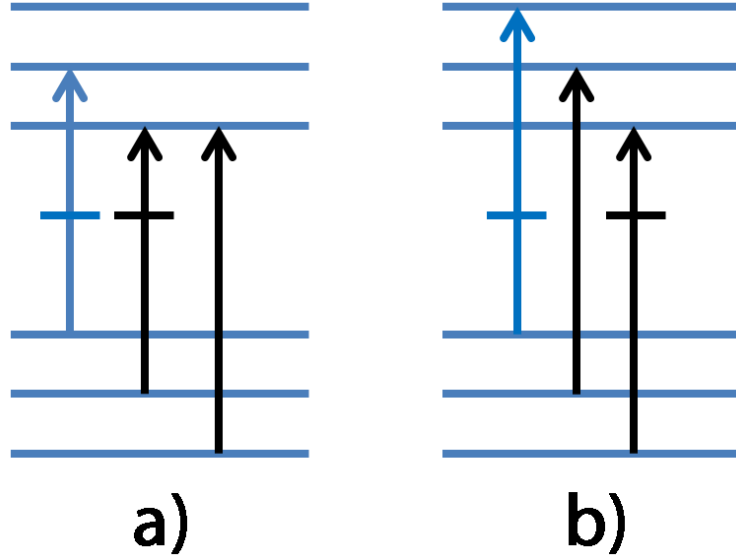


Figure 2.1: **a)** A Λ -type configuration of two lasers in a triplet-triplet configuration **b)** A Π -type configuration of two lasers in a triplet-triplet configuration at a moderate magnetic field strength. The vertical arrows denote laser-driven transitions: the black arrows are the transitions belonging to the Π and Λ pumping schemes. The blue arrows denote the third transition necessary to address all ground states. The horizontal bars on the arrows denote transitions of equal wavelength.

From the transitions in figure 2.1 we can expect to notice spin pumping varying with two-laser detuning as a result of Zeeman splitting (see appendix [B]) of the three different spin projections for a spin triplet. The perturbation of an external uniform magnetic field is given by the Zeeman Hamiltonian of the spin operator \vec{S} in a magnetic field \vec{B} :

$$\hat{H}_z = g_e \mu_B \vec{B} \cdot \vec{S} \quad (2)$$

Where g_e denotes the Landé factor for electrons and μ_B is the Bohr magneton. Spin pumping features belonging to a Λ -configuration are able to show CPT and Π -features are not, since no destructive interference of two laser fields can occur when coupling to two different excited states. Spin pumping lines can occur and disappear as a function of magnetic field, since at certain \vec{B} two transitions could be both exactly resonant to one laser frequency, whereas these transition frequencies diverge if \vec{B} is increased or decreased in amplitude. The angle of the growth axis (which is the direction of the dipoles of the PL2 divacancies) of the sample to the orientation of the magnetic field, 33° , was chosen such that there is significant overlap between two transitions, giving rise to spin pumping schemes as shown in figure 2.1. The strength of the spin pump features is dependent on the spin overlap between the levels defining the transitions underlying the spin pump scheme. Dephasing rates between ground state levels is very small in SiC divacancies, due to small wavefunction overlap between these levels.¹⁹ Dephasing processes and transition strengths could cause potential spin pump lines to be much weaker than others, just as ISC can.⁷ Additionally, due to Zeeman splitting, one can expect lines to appear and disappear as a function of magnetic field. Transition frequencies can be identical for particular magnetic field strengths, whereas they can be different from each other at other magnetic field strengths, as shown in figure 3.4.

2.6 Optical bleaching

When optically driving transitions in the ZPL range it is found that, once powers are sufficiently high, absorption by divacancies in a given frequency range can disappear by the effect of spectral hole burning.²⁰ The process of optical bleaching in V_{SiC} is found similar to that in NV-centers: electrons residing in the divacancy can be excited to a level within the conduction band of the surrounding SiC or a hole excited from the divacancy to the valence band of the surrounding SiC can change the charge state of the divacancy.²¹ The other charge state has a different electronic structure and the applied laser field is no longer resonant with a transition present in the SiC sample and photon absorption decreases, which is the spectral hole that is created in the absorption spectrum. In divacancies in SiC, all conditions necessary for spectral hole burning by optical bleaching are met.²⁰ The bleached, dark state is more negatively or positively charged relative to the initial charge state, depending on the underlying bleaching process.

It has been found that strong illumination within a short wavelength range (optimal at 770 nm) is able to restore the complex to its old charge state, referred to as repumping. In NV^- defects in diamond, bleaching to NV^0 is a two-photon process (a double hole excitation) and the repump process (a double electron excitation) is also a two-photon process. However, also two other single photon electron excitations could cause the charge state to alter (see figure 4.1).

Time traces of the bleaching process are able to unveil several characteristics of the process. If this two-photon process, as bleaching in NV-centers is, does not go via an intermediate stable level, one expects a very low power to bleach extremely slowly, since the probability two photons occur very fast after each other, is very low. Hence, the bleaching process will be one that behaves quadratically in laser intensity. If it is a one-photon process instead, it will behave linearly in laser intensity.

Bleaching is not solely a problematic issue in divacancies, since it could also be used to reduce effective inhomogeneity. Due to strain in the sample the levels and transitions are inhomogeneously broadened as explained in section [2.4]. To reduce inhomogeneous broadening issues for optical spin manipulation, one could bleach a part of the inhomogeneously broadened ensembles to another charge state, to arrive at a narrower, less-broadened ensemble of divacancies. Next to that, by understanding the process of bleaching from its transition frequencies as shown in figure 1.1, one can infer the relative position of the divacancy within the band gap of the surrounding SiC.

3 Exploring the Excited State Structure by Magneto-spectroscopy

In order to determine level structure the excited state of the deep-lying defect, a two-laser experiment was designed, with one of both lasers was chopped with a 270 Hz frequency. The transmission signal is governed by absorption and emission due to resonant laser fields. The persistent pumping of electrons to different spin levels is detected by a lock-in technique which is discussed in section [3.2]. Spin pumping occurs for the requirements named in section [2.5], which is analyzed for a simple triplet-triplet model in section [4.2.1].

In section [4.1], magneto-spectroscopic features are identified and spin pumping features have been categorized. In section [4.2.1], the expected spin pumping features for a simple triplet-triplet model without restrictions are shown and compared in section [4.2.2] to the data of [4.1]. In section [4.3], the validity of a manifold excited state is tested by the influence of bleaching between features and three hypotheses for the excited state structure will be posed. Section [4.4] discusses the observation of asymmetric CPT in a spin pumping feature.

3.1 Spin pumping features by magneto-spectroscopy

By magneto-spectroscopy we obtained surface plots for three different carrier frequencies. The features vary with magnetic field due to the specific Zeeman splitting of levels belonging to transitions that engage in spin pumping. These results are given in figure 3.1, where the darker the feature is, the stronger the lock-in signal. Figure 3.1c) names the features, where Λ -features denote features in a Λ pumping scheme, since they show CPT, and Π -features denotes features belonging to Π spin pumping schemes.

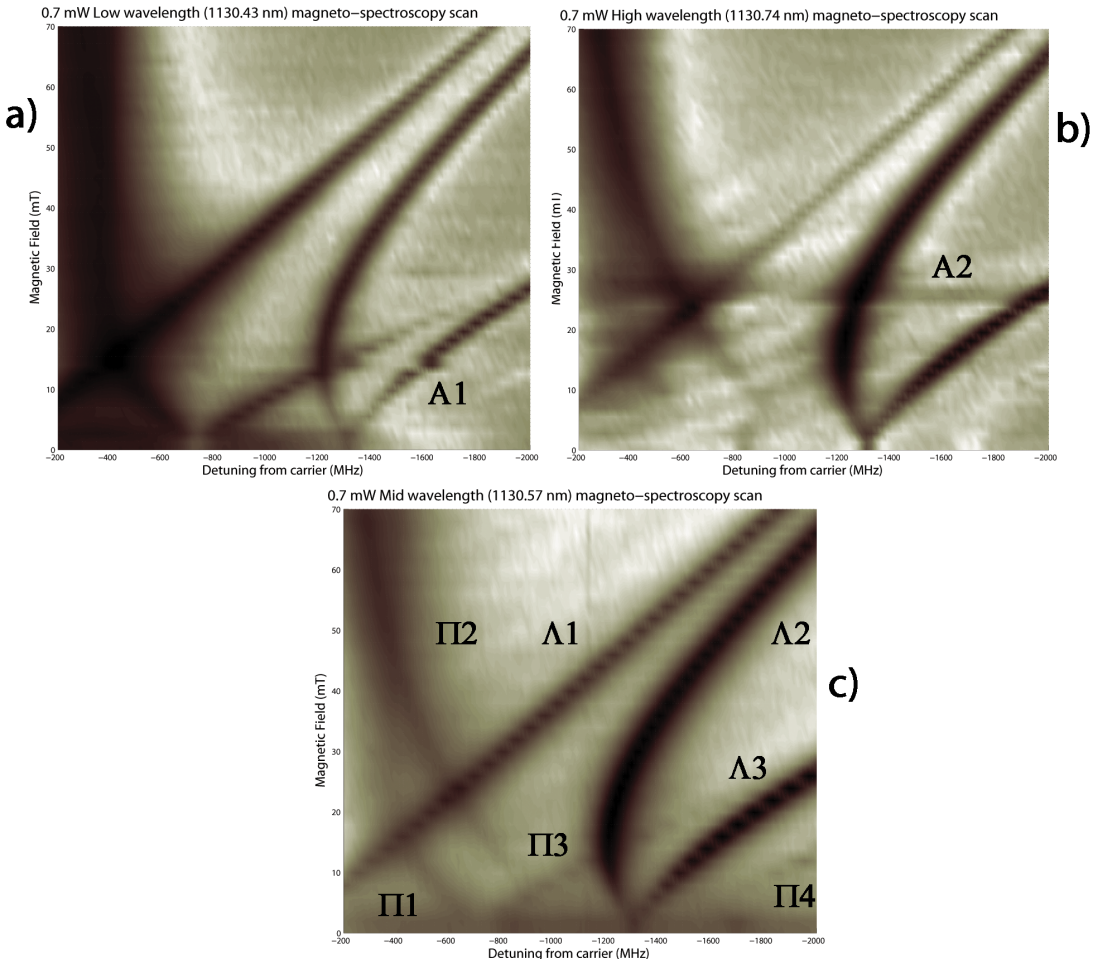


Figure 3.1: Magneto-spectroscopic features at 4.2 K between 0 and 70 mT at a two-laser detuning between -200 and -2000 MHz from a carrier wavelength of a) 1130.43 nm, b) 1130.74 nm and c) 1130.57 nm. Λ -features are features showing CPT, Π -features are other spin pumping features and A -features are shown to be artefacts of this specific measurements. Moderate powers of 700 μ W and 800 μ W were used for both laser fields to retrieve these scans. The darkness of the surface plot is the logarithmic lock-in signal (see section [3.2]) in arbitrary units. The higher the lock-in signal, the more absorption of both laser fields by electrons has occurred.

From these plots, features $\Pi 1$, $\Pi 3$ and $\Lambda 1$ are clearly more present at the low end than at the high end of the carrier wavelength, where $\Pi 2$, $\Pi 4$, $\Lambda 2$ and $\Lambda 3$ are dominant at the high end of the carrier wavelength. Both carrier wavelength and frequency are used in this section, depending on the convention, to denote the middle frequency of a two-laser experiment to probe the transitions in the material close to the ZPL of the PL2 divacancy.

The horizontal features, $A1$ and $A2$ at the plots have been checked and are artefacts that showed up only during a single scan, attributable to magnetic field instabilities. Features show interactions and some features appear and disappear as a function of magnetic field. From figure 3.1a), we see line $\Lambda 2$ to increase its intensity suddenly after it crosses line $D3$. This could be a coincidence, but when the sample was mounted under an angle of 57° to the magnetic field, similar interactions were observed. Features appearing and disappearing can be understood in the simple model by transitions starting to overlap and to diverge as explained in section [2.5].

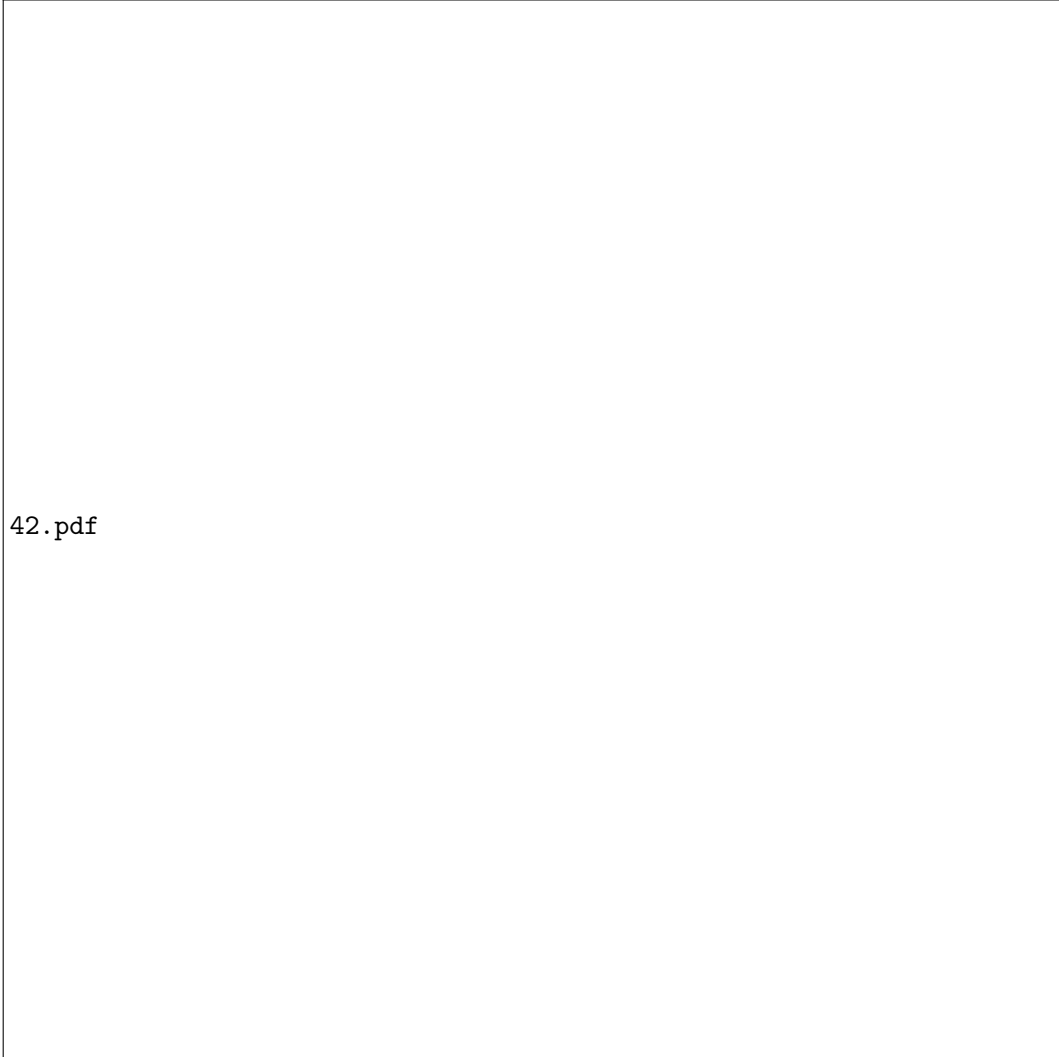


Figure 3.2: Magneto-spectroscopic features at 4.2 K at 9 mT for a two-laser detuning between -200 and -2000 MHz and carrier wavelengths between 1130.26 nm and 1130.85 nm. The brightness of the surface plot is the lock-in signal (see section [3.2]) in arbitrary units. The higher the lock-in signal, the more absorption of both laser fields by electrons has occurred. This figure is a cross section of figure 4.1 at 9 mT over different carrier wavelengths.

From figure 3.2, we confirm the magneto-spectroscopic features to belong to two sets centered at different carrier wavelengths: one set is centered at a wavelength of 1130.5 nm and the other is centered at 1130.61 nm. Hence, these two sets of features have a slightly different energy spacing and therefore a slightly different ZPL. This scan was performed at 9 mT: at this field strength all features were clearly distinguishable, as shown in figure 3.1c). Both sets show a different amount of spin pumping features and different features. Features $\Lambda 1$, $\Pi 1$, $\Pi 3$ belong to the low carrier wavelength set and $\Lambda 1$, $\Lambda 2$, $\Pi 2$ and $\Pi 4$ belong to the high carrier

wavelength set. The center of those sets are separated by a splitting of around 35 GHz. Next to this, we observe that both sets show rather wide inhomogeneous broadening of around 50 GHz.

The high carrier wavelength features, originating from a -1.305 GHz detuning at **0** magnetic field, which is equal to the crystal field D-parameter of the ground state, could be explained by a triplet excited state (see section [4.2.1]). The fact that these features are originating from approximately a -1.305 GHz detuning is strong evidence that these features are indeed part of the ground state of the neutral PL2 divacancy in SiC. Two of the low carrier wavelength features originate from approximately a -740 MHz detuning. The diagonal line through the origin also belongs to the low carrier wavelength. By observing spin pumping features not showing CPT, there need to be at least two excited states present in the low carrier wavelength set. Here, the suspicion is raised there might be two sets of excited states, either belonging to a single type of defect or to two different defects.

From figure 3.1, next to the features identified as spin pumping features, a background signal between the features can be identified. This background signal showed even to be stronger for a mounting angle (see section [2.5]) of 57°. From a rate equation model, it has been observed that strong background signal is possible, by tweaking ISC and transition strength parameters. A rate equation model models the influence of absorption by applied laser fields and emission on electron population in a specific electronic structure. The model outputs a steady state solution of the electronic levels their population and the belonging emission as a function of two-laser detuning and magnetic field. Hence, the above noise background of figure 3.1 does not have to mean an other mechanism is present.

3.2 Spin pumping features in a simple triplet-triplet model

3.2.1 Triplet-triplet model

In this section, the model assumptions of no ISC and no forbidden transitions and its implications for the electronic structure and expected spin pumping features of a triplet-triplet model are shown. NV-centers in diamond possess a similar group theoretic symmetry ($C3v$) as c-axis divacancies in SiC, which leads to manifold triplet excited states and singlet states.¹³ Therefore, it is expected that a double orbital triplet excited state could be underlying spin pumping features. The observed magneto-spectroscopic features can not occur due to spin pumping in singlet levels solely, since singlet levels do not split by magnetic field and therefore no \vec{B} dependent splitting could occur.

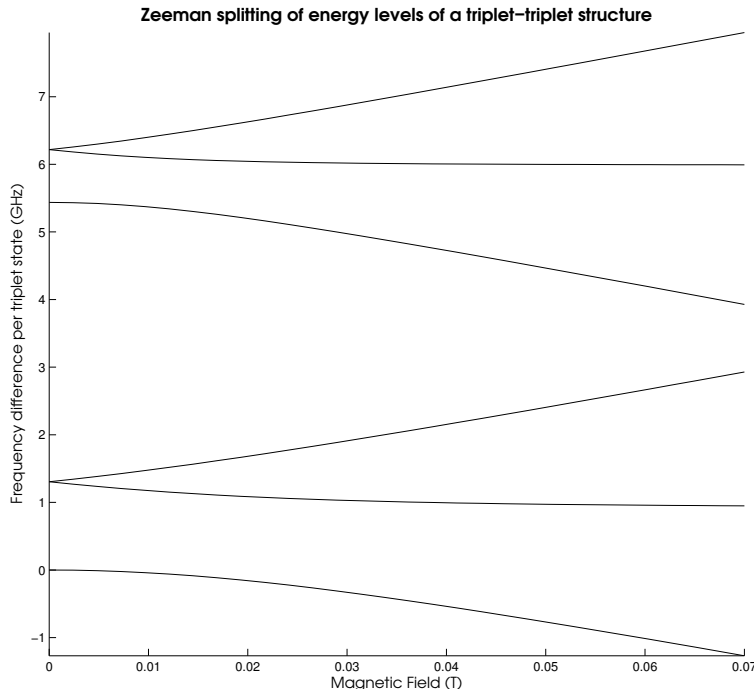


Figure 3.3: Electron energy level structure as a function of magnetic field for $D_e = 0.78$ GHz and $E_e = 0$ GHz at a 33° angle between the sample c-axis and the applied magnetic field. The spin projections $m_s = 1$ and $m_s = -1$ are degenerate at **0** magnetic field. The separation in frequency between the upper and lower triplet is arbitrary. The actual separation between those triplets equals the ZPL, which are shown by experiment in figure 3.2.

The energy levels of an orbital triplet is given by the solution of the spin Hamiltonian in appendix [B]. The calculation of the level structure from the Hamiltonian is given by Zwier *et al.* (2015). From the Hamiltonian one can compute the energy levels, possible transitions and the spin pumping features, given the criteria from section [2.5]. All plots are provided for ground state parameters $D_g = 1.305$ GHz and $E_g = 0$ GHz and excited state parameters $D_e = 0.78$ GHz and $E_e = 0$ GHz, where the first three are given in literature.⁶ The angle between the sample its c-axis and the magnetic field direction is 33°.

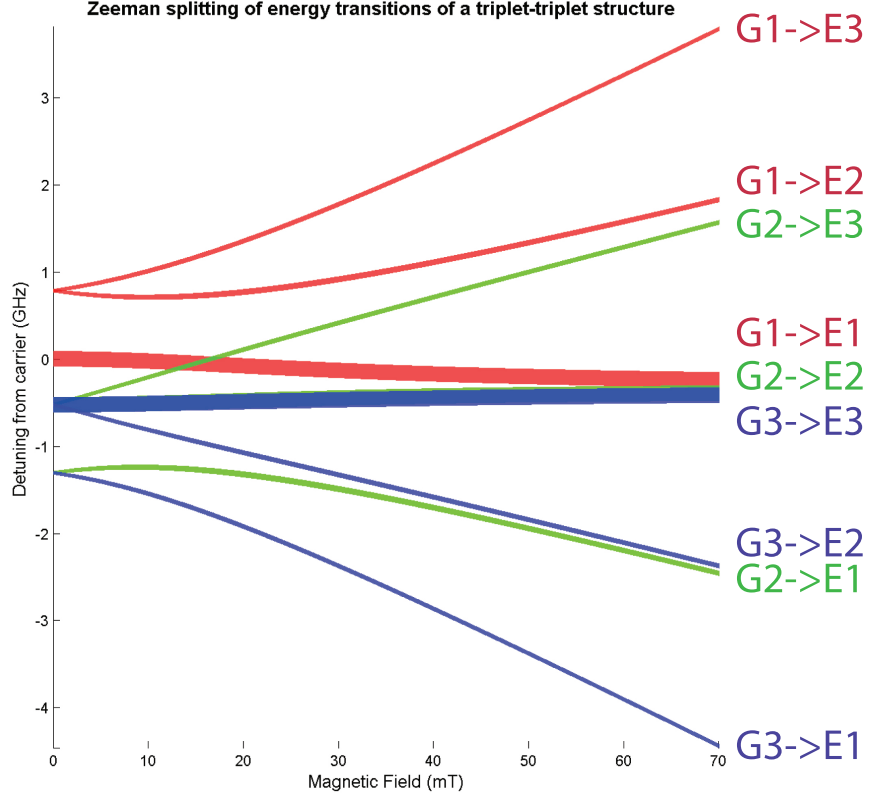


Figure 3.4: The 9 possible transitions, normalized to carrier frequency, for the level structure of figure 3.3 as a function of magnetic field for $D_e = 0.78$ GHz and $E_e = 0$ GHz. The levels involved in these transitions are shown on the right, where ‘G’ and ‘E’ are the ground and excited state respectively and ‘1’, ‘2’, ‘3’ are the lowest, middle and highest level of a triplet respectively. Red lines are transitions resonant to the lowest ground state, green ones to the middle ground states and blue ones to the highest ground states.

The spin pumping features of figure 3.5 are given by the criterion that all three ground state transitions need to be resonant with a laser present to resemble spin pumping. This occurs when two transitions overlap in figure 3.4, since there are two lasers present. These transitions are given by the double triplet level structure of figure 3.3. We observe 6 spin pump features, all in pairs of two, which can be understood by figure 3.4: two close lying lines are belonging to two transitions very close to each other and these form a spin pump feature with a third transition.

3.2.2 Fit of magneto-spectroscopic features to model

In order to determine the excited state structure parameters (D_e and E_e) for a triplet that can resemble certain spin pumping features, a level and transitions model given the ground state is estimated in section [4.2.1]. By comparing potential spin pumping features from this model and the actual features observed (section [4.1]), one can identify features their underlying transitions and infer whether the triplet-triplet electronic structure is reasonable.

Before the suspicion of two different sets of defects of section [4.1] was raised, an attempt was made to fit all features to a single triplet excited state. However, no set of D and E parameters was able to show all these features simultaneously. Nevertheless, since the suspicion was raised that both defects were belonging to different sub-ensembles, which is confirmed in section [4.3.1], we will try to estimate the parameters for the high wavelength set of features (all features originating at a -1305 MHz detuning in figure 3.1).

The result of this analysis is shown in figure 3.5, which is not able to explain the features observed in figure

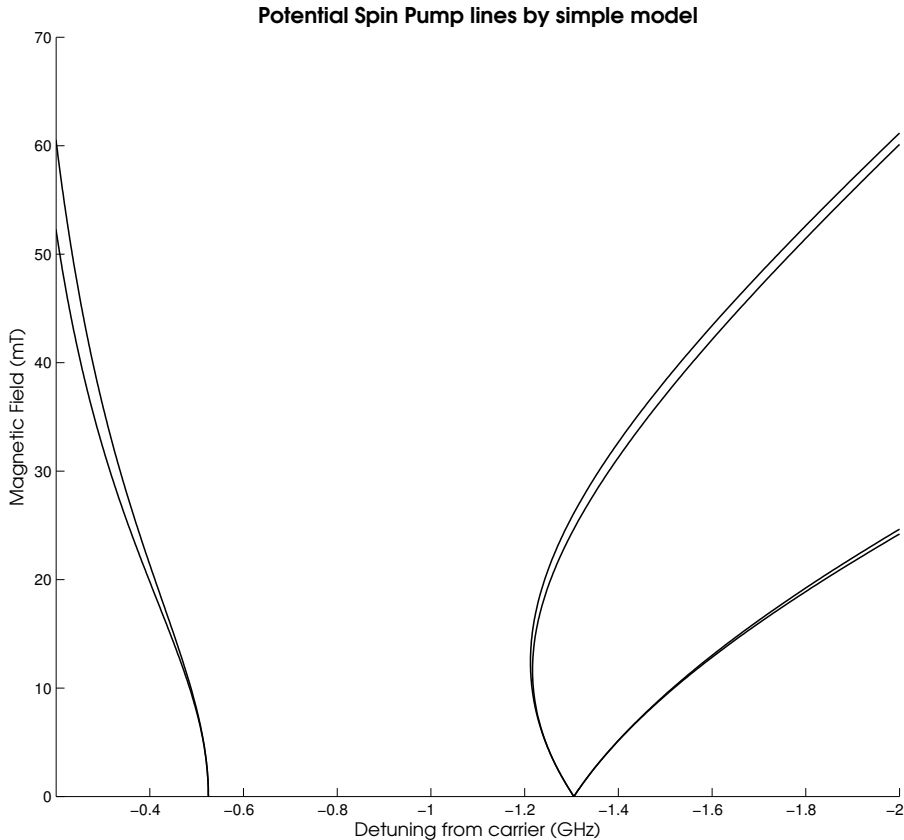


Figure 3.5: *Spin pumping features arising from the level structure of figure 3.4 as a function of magnetic field for $D_e = 0.78 \text{ GHz}$ and $E_e = 0 \text{ GHz}$. Only features that -in a part of the magnetic field range- obey the criterion of all ground states resonant to a laser field present are shown. This criterion is equivalent to that of two overlapping transitions in 3.4, that form a spin pump feature with a third transition resonant to a ground state level not involved in the two overlapping transitions.*

3.1b). Although section [4.2.1] discusses only the possible spin pumping features for a single value for both D_e and E_e , other values of these parameters are not able to resemble different features that could be those of figure 3.1. The features do not differ much for different D_e and D_e is similar from literature (0.78 MHz).⁶ Next to that, changes in E_e only shifts the origins of features identical to $\Pi 2$ and $\Pi 4$ in figure 3.1 severely, that are not spin pumping features according to the requirement of resonant ground states in the model of section [4.2.1] and therefore not shown in 3.5. Hence, if the simple model is able to show to closely resemble the experimental spin pumping features, the excited state parameters can be slightly different from those in section [4.2.1]. Besides, the features $\Lambda 1$ and $\Lambda 2$ are not shifted by changes in excited state parameters. The reason for that is that Λ -configurations are only resonant to a single excited state and therefore two-laser experiments show to be independent of excited state.

In figure 3.5, we observe two features that are not present in the magneto-spectroscopic data (transitions $G1 \rightarrow E2$ and $G2 \rightarrow E2$, $G1 \rightarrow E2$ and $G3 \rightarrow E3$) and we miss two features in figure 3.5 that are very similar to two magneto-spectroscopic features ($\Pi 2$ and $\Pi 4$). These features are attributed to transitions $G1 \rightarrow E2$ and $G2 \rightarrow E3$ ($\Pi 2$) and $G1 \rightarrow E3$ and $G3 \rightarrow E2$ ($\Pi 4$) in the simple model, which do not satisfy the condition of all three ground states resonant to a transition to be observed as spin pumping lines. Therefore, the simple triplet-triplet model can not be underlying the high wavelength group of figure 3.1.

Using these missing features, ignoring ISC for now, one can attempt to tweak the transition strengths as such that they *do* show the features. However, for $\Pi 4$ to occur, transition $G3 \rightarrow E2$ should be forbidden, but this transition gives rise to line $\Pi 2$. Therefore, only forbidden transitions are not able to explain these spin pumping features. Allowing for strong ISC to particular ground state and considering a rate equation model as described in section [4.1] could bring us closer to a solution, but it should consist of fitting 6 parameters (all interactions between the six levels and a intermediate singlet level). Therefore it is hard to arrive at a model explaining the 4 features originating at -1305 MHz detuning, although it seems reasonable such a set of features is due to a triplet-triplet electronic structure. In a similar way, the low wavelength set of features

can be fitted to a triplet excited state. However, these yielded different excited state parameters than for the high wavelength set and also require ISC and differing transition strengths to possibly explain the observed features.

3.3 Excited state structure

3.3.1 Independence of two sets of spin pumping features

The two sets of features at different carrier frequencies observed in figure 3.2 could belong to one inhomogeneously broadened ensemble of similar defects with two excited states split by around 35 GHz. These excited state should have a different electronic levels, since they show different spin pumping features with the same ground states. However, those two sets could belong to two different physical ensembles of defects as well. To determine whether the spin pumping features in figure 3.2 originate from different physical defects or from the same defects, one can perform spectral hole burning by bleaching one of the two sets. If both sets belong to the same physical defects and hence to the same electronic structure, bleaching one set should also bleach the other set, since the lock-in signal strength is related to the amount of resonant defects present.

If an electronic structure has a double triplet excited state and both excited states their levels are inhomogeneously broadened by strain in a similar way, one expects the hole burned in the middle of one excited state's feature to be present in the other excited state's feature. However, if the assumption of similar broadening by strain is not valid, the weaker this correlation is, the broader the bleaching hole that can be observed in the non-bleached set of defects their features. Hence, at very low correlation no sharp dip in absorption can be seen by a scan over a feature, but a general drop in absorption over the entire feature.

Spectral hole burning parts of features by bleaching can be most optimally performed at high laser intensities, whereas scanning the features to check whether there is a spectral hole should be performed with sufficiently low laser fields to prevent bleaching.

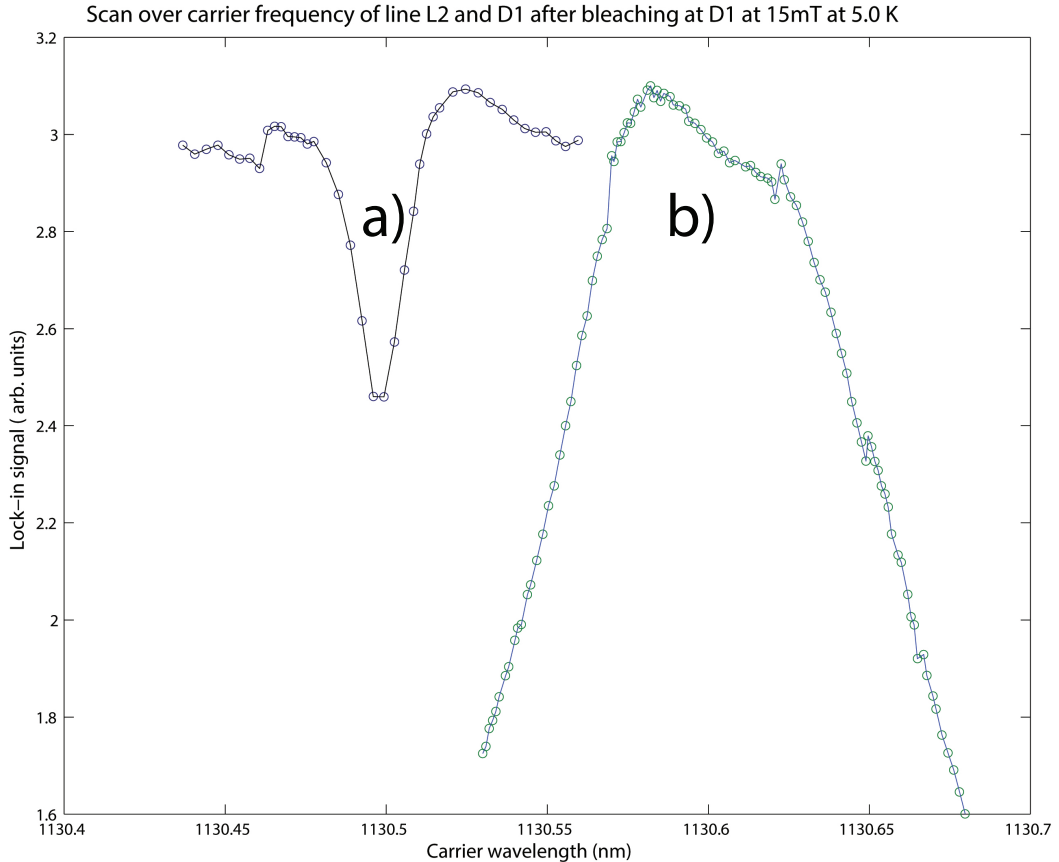


Figure 3.6: a) A scan over feature $\Pi 1$ as a function of carrier wavelength after bleaching a spectral hole at 1130.5 nm for 5 minutes at high power: It shows a clear spectral hole of around 10 GHz wide. This non-invasive scan was performed at 300 nW intensity for the scan and probe laser. b) A similar scan over feature $\Lambda 2$ was performed. No sharp spectral hole is observed in the $\Lambda 2$ feature. These scans were taken at 5.0 K.

Figure 3.6b) clearly shows that bleaching the low wavelength set of defects, causing a bleaching dip of around 10 GHz wide, did not show a sharp bleaching hole in the other set. Therefore, the sets of features do not belong to the same physical defects or the assumption of strong correlation between the inhomogeneous broadening of both excited states does not hold. However, it has not been tested yet whether there was a broader drop in absorption.

3.3.2 Excited state structure hypotheses

The two sets of defects originating from different carrier wavelengths, found in figure 3.2, suggest that there are two sets of features at different carrier frequencies. Candidate hypotheses that could explain two sets of features for these observations are the manifold excited state as in NV-centers (first hypothesis), the existence of a second deep-lying defect with a transition frequency that is close to that of the PL2 divacancy (second hypothesis) and an exotic strain-induced non-continuous effect that alters the electronic level structure and ISC and/or transition strengths (third hypothesis).

The first hypothesis could be rather easily rejected by the experiment of section [4.3.1]. However, although no sharp bleaching hole occurred, the hypothesis could still be tested by comparing the features of figure 3.6 before and after bleaching a spectral hole in a feature of the other set. Moreover, the interaction of two features observed in figure 3.1, both from a different set, poses some evidence for this hypothesis. An interaction between two features in magneto-spectroscopy can be understood by many transitions being close to each other, causing dynamic population effects to show a different signal from the summation of the two separate signal.

The second hypothesis is also affected by this interaction: interacting features are not expected from two different defects with unrelated electronic structures. Moreover, if the bleaching test for the first hypothesis shows a dependence of both sets of features, this hypothesis is very unlikely. The hypothesis of an impurity could be tested by using different samples having different impurity concentrations and comparing relative magneto-spectroscopic features their strength. The more colour centers present, the stronger absorption by resonant transitions and the stronger the lock-in signal in two-laser interactions is. Hence, if the low carrier wavelength set their features its relative strength to the other set increases with impurity concentration, the low wavelength features can be attributed to the added impurity atom. However, to test whether both sets of features are due to divacancies in SiC, a similar test for absolute feature strength could be performed. If both sets of features show an increased lock-in signal when more divacancies are present, these sets should be both attributed to divacancies.

The third hypothesis suggests that ISC and transition strengths depend on strain within the sample in a discontinuous way: there are two configurations with a slightly different ZPL and different ground and excited state splittings. This strain dependent configuration and ISC and differing transition strengths could cause the magneto-spectroscopic features to show in the fashion observed. If the bleaching test for the first hypothesis shows a dependence of both sets of features and the interaction between two sets of features, this hypothesis is very unlikely. A way to check for this hypothesis is by performing magneto-spectroscopy at another place on the sample or by straining the sample intentionally and check whether the relative signal in magneto-spectroscopy of both sets changes. If the relative signal changes, there is proof that strain indeed is able to change the amount of divacancies in a certain configuration is dependent on strain.

If one of these three processes is underlying the observed spin pump features, still some issues have to be solved to fully understand the features observed in section [4.1]. For the low wavelength set of magneto-spectroscopic features, the features can be explained by features from a triplet-triplet model with different parameters. Just as with the other set, one could not find the correct splitting parameters and transition strengths that exactly yield the observed features in a triplet-triplet model. However, by ISC and different transition strengths these features could be observed, but these can't be spin pumping features without ISC and transition strengths. If a particular hypothesis is posed, one can use a rate equation model, as named in section [4.1], for that particular electronic structure and fit its splitting, ICS and transition strength parameters to the features that most closely resemble that of figure 3.1.

3.4 Asymmetric CPT in c-axis defects

In this section, Coherent Population Trapping was investigated for c-axis defects by a scan over a spin pumping feature at high control and probe laser powers. However, the sharp and narrow drop in absorption due to CPT did not occur in the middle of the Λ 2-line, as shown in figure 3.7. A reasonable explanation to this phenomenon, that did not occur at a different mounting angle of 57° and hence a different magnetic field direction, is the occurrence of multiple features close to each other.⁷ If one of these features is actually a

Λ -line and the other is not, the CPT feature will occur in an asymmetric fashion. A different magnetic field angle is able to alter the level structure by a different Zeeman splitting, see equation (2).

The feature occurring at the high absolute detuning end of the feature corresponds to a spin pumping scheme identical to that of the Λ -system within the Lorentzian linewidth of the transition since the CPT dip is a bit wider than 30 MHz. The other feature is a feature that does not show CPT and is probably a Π system, which we call the ‘brother’ of the CPT feature. Both the lambda and the ‘brother’ line need each other to show spin pumping in the simple triplet-triplet model of section [4.2.1]. If both laser fields are resonant with the transitions forming the brother feature, CPT will not occur due to the Λ -system being slightly off-resonant with the small bandwidth in which CPT occurs. Therefore, two features can be close to each other in magneto-spectroscopy plots, in which a transverse scan over this feature shows CPT in an asymmetric way. Moreover, the nomenclature Λ 2 is rather misleading since this feature actually consists of two features, originating from a Π and a Λ spin pumping scheme.

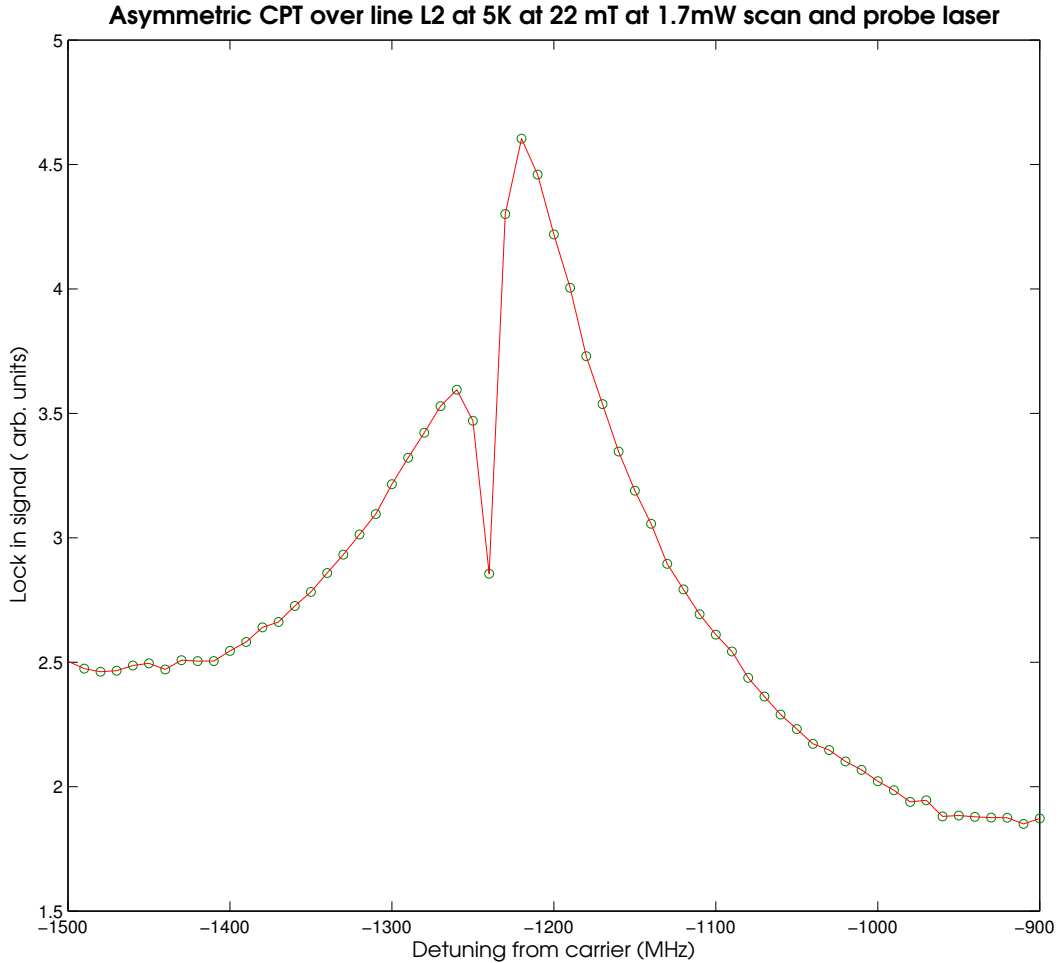


Figure 3.7: Asymmetric CPT in feature Λ 2, shown by a scan over detuning at 9mT at 5.0 K. The two applied laser fields had intensities of 1.4 mW each. The CPT feature occurs at the high absolute detuning side of the feature. The width of the Λ 2-feature is around 200 MHz and the CPT dip is at least 30 MHz wide.

The conclusion of asymmetric CPT also confirm that by neglecting differing transition strengths and ISC, one can not explain the magneto-spectroscopic features. Two magneto-spectroscopic features show no precise overlap in magneto-spectroscopy plots, which is concluded from asymmetric CPT, since the suspected underlying transitions G2->E2 and G3->E3 (see figure 3.4) do not overlap. Moreover, the maximal width of the spin pump feature Λ 2 is 200 MHz, which exceeds the linewidth of 100 MHz. Because these two features do not need the overlap of their underlying transitions to show magneto-spectroscopic features, both of the features can’t be spin pumping features in the simple model of section [4.2.1].

4 Optical Bleaching in C-axis Divacancies

As discussed in section [2.6], bleaching alters the charge state of the divacancy by donating to or accepting an electron from the SiC environment. The interesting question to be addressed here for SiC divacancies is whether the bleaching process is a one- or two photon process. From this, the pathway of the bleaching process can be determined and the position of the divacancy within the band gap can be inferred. In section [5.1] temporal absorption data for bleaching is discussed, a fitting method of a functional form is proposed in section [5.2] to investigate the power to which laser intensity influences the exponential decay constant, a general comparison between one- and two photon processes given the functional shape is shown in section [5.3].

Considering the simplified energy band model for divacancies in section [2.6], there are several possibilities for one- or two photon processes to a level either in the valence or conduction band of the surrounding material. Figure 4.1 denotes five possible bleaching processes, when no electrons reside in the excited states and no holes reside in the ground states. Three processes are single photon processes, two are processed requiring two photons. Each of these processes can be characterized by either hole excitation or electron excitation.

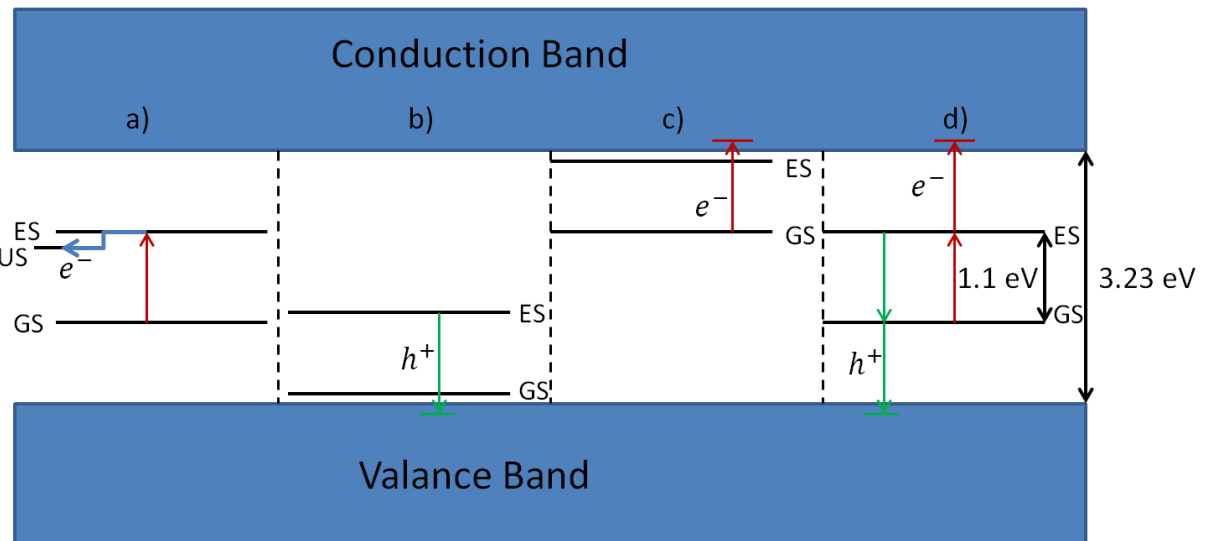


Figure 4.1: Energy band picture of the proposed bleaching processes, where 5 different processes are distinguished: a) An electron excitation from ground to excited state, followed by a crossing to another level denoted as the Unknown State (US), which can be any energy level present in the material surrounding the divacancies. b) a single hole excitation, c) a single electron excitation, d) a double electron and double hole excitation to either the valence or conduction band could switch the charge state of the divacancy. A hole excitation would give rise to a negative charge state, whereas an electron excitation would give rise to a positive charge state.

As stated in section [2.6], a single photon process is expected to exponentially decay by a decay constant that is linear in intensity and a two-photon process is expected to exponentially decay by a decay constant that is quadratic in intensity. However, if this model for the electronic band structure is oversimplified, multiple other pathways in the electronic structure could cause charge state switching when considering multiple excited states and singlet states, as discussed in chapter [4].

4.1 Temporal bleaching traces

Optical bleaching data was retrieved by illuminating the SiC sample as described in section [3.1] in the resonant charge state for a certain period of time for different intensities at a wavelength of 1130.6 nm. The repump laser was switched off during this procedure and it was observed bleaching could last for hours. The relative absorption of bleaching on the ZPL was recorded for several minutes (depending on the laser intensity). If the charge state of the divacancy is altered to a non-resonant charge state, no light is absorbed and the absorption signal drops, as shown in figure 4.2. Next to bleaching, also the repump process was considered. A strong pulsed laser of 770 nm is able to repump by illuminating the side band of the transition back to the old charge state. The range of frequencies repumping is more or less present is relatively large. One finds that the repump process is generally faster, and hence more efficient, than the bleaching process. Repumping at

$125 \mu\text{W}$ had around the same percentage effect to transmission as bleaching at $3500 \mu\text{W}$ had to absorption. This can be attributed to a higher likelihood of absorption by the repump process.

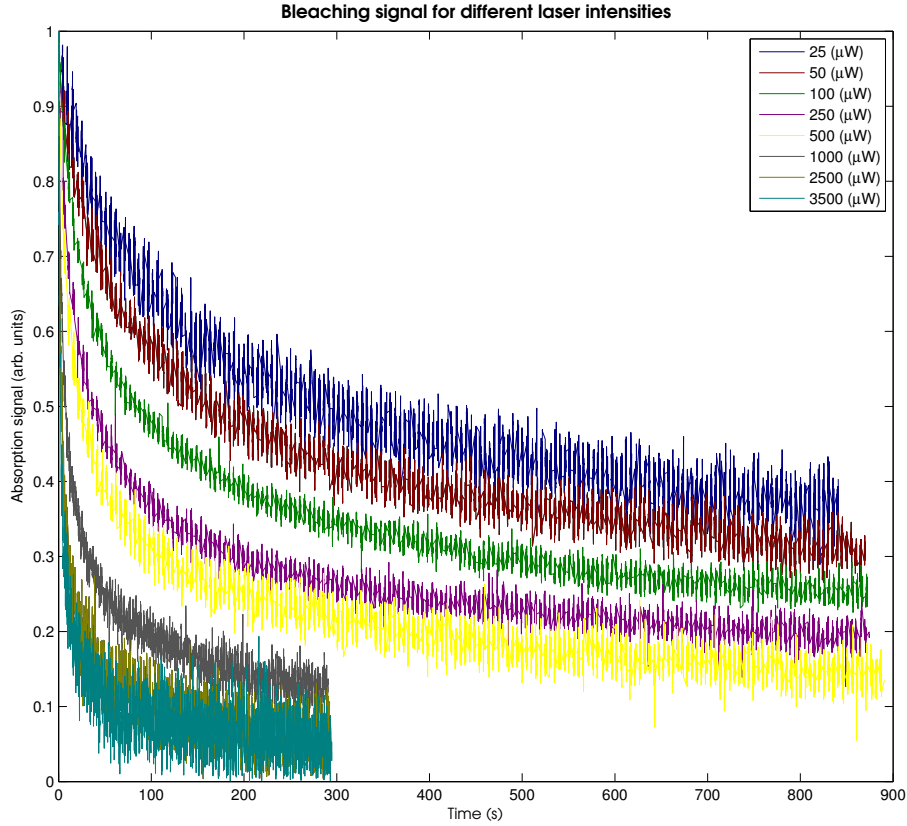


Figure 4.2: Bleaching traces for several intensities at 20.0 K . Both the pace of the absorption decay and the shape of the decay of the absorption signal depends on the laser intensity. At low powers 10 minutes of bleaching only reduces the signal only little more than half.

The traces of figure 4.2 are rather noisy, although the trends are clear. A higher intensity clearly causes the divacancies to bleach faster. A problem with the high intensities traces could be that the signal does not decrease to zero within the time range considered, due to a noise floor as discussed in section [5.3.1]. Therefore, the trace is flattened out if time increases, which causes the trace to be different from actual bleaching alone. The traces for the higher intensities show a kink in their path, showing an initially fast drop and a slower process after the kink: this could be a result of a noise floor.

4.2 Bleaching model

A functional form was derived to fit the bleaching process to a formula describing bleaching likelihood governed by transition linewidth and laser spatial intensity distribution. It is supposed bleaching is an exponential phenomenon, since its rate (over time) depends proportionally on the currently present population in the initial charge state, which is reduced due to the bleaching itself. Hence we write:

$$y \propto e^{-\gamma t} \quad (3)$$

Where y is the absorption signal from the defect its initial neutral charge state and γ is the exponential decay factor specified by:

$$\gamma = kI^m \quad (4)$$

Where k is a constant which captures how likely a divacancy is bleached when a particular effective intensity is present. k can be influenced by for example the density of divacancies. The effective laser intensity distributed over transition linewidth and laser spot can be specified by:

$$I = I_0 G \mathcal{L} \quad (5)$$

Note that any intensity attenuating effects in the sample, caused by absorption, are neglected. The Gaussian is the approximate intensity distribution of the laser spot in the sample, specified by a Full Width at Half Maximum (FWHM) of approximately $100 \mu\text{m}$. The Lorentzian \mathcal{L} defines the likelihood of transition for a transition with a particular frequency. The Lorentzian here is normalized around its central frequency. The Gaussian distribution is given by:

$$G(r) = \frac{1}{\sigma\sqrt{2}} e^{-\frac{1}{2}\left(\frac{r-\mu}{\sigma}\right)^2} \quad (6)$$

Where the standard deviation as a function of the FWHM is given by: $\sigma = \text{FWHM}/(2\sqrt{2\ln(2)})$ And the Lorentzian is given by:

$$\mathcal{L}(f) = \frac{1}{\pi\delta\left(1+\left(\frac{f}{\delta}\right)^2\right)} \quad (7)$$

Where δ is half the FWHM of the transition linewidth Lorentzian, which is estimated to be 100 MHz. The essential physical parameter in the Lorentzian is m , which is the power of the intensity in the γ -factor. If the bleaching process goes via two photons, the likelihood of a defect bleaching will be quadratic in the applied laser power and $m = 2$. Both the Gaussian and Lorentzian distribution are simplified by dividing their functions within two FWHM distance from the middle in 14 pieces to allow for a numerical approach. It was found that further refining these distributions did not alter the traces of figure 4.4, 4.5 and 4.6 much. The form derived needs to be integrated over spatial laser distribution and frequency linewidth distribution, ignoring laser linewidth, which is small, as described in section [3.1]. Using a radial coordinate frame for the spatial distribution (the intensity is radially symmetric) and the given Lorentzian frequency linewidth distribution, we obtain:

$$y = 2\pi \int_{-f'}^{f'} \int_{-r'}^{r'} r e^{-k(I_0 G(r) \mathcal{L}(f))^m t} dr df \quad (8)$$

Which is approximated by a double Riemann sum:

$$y \approx 2\pi \sum_{r=-r'}^{r'} \sum_{f=-f'}^{f'} r e^{-k(I_0 G(r) \mathcal{L}(f))^m t} \Delta f' \Delta r' \quad (9)$$

Where y denotes the absorption signal. When plotting, we normalize the summation since the bleaching signal is normalized as well. Hence the normalization of the obtained formula refers to the fraction of divacancies in the initial, resonant charge state.

4.3 Results

4.3.1 Fit of traces to model

We now try to fit the bleaching traces with the data available to the functional form derived in section [5.2]. This is initially performed by making surface plots displaying the error of the fit relative to the data for different k and m values. After refining the range of k and m values, figure 4.3 was obtained. An interesting feature we observe from figure 4.3 is that the error shows a canyon of small fit errors in k, m -space, hence the actual value of m and k could be slightly off. However, at the end points of this canyon fitting errors were more than twice as big as the minimum. Moreover, for lower or higher values of m the error increases tremendously.

Surface plots of the error of the fit to the signal were performed for 1 mW laser power incident on the SiC sample and these showed a best fit for $m=0.97$ and $k=4.36$, as shown in figure 4.4.

Error of the bleaching signal fit for different parameters k and m at 1mW

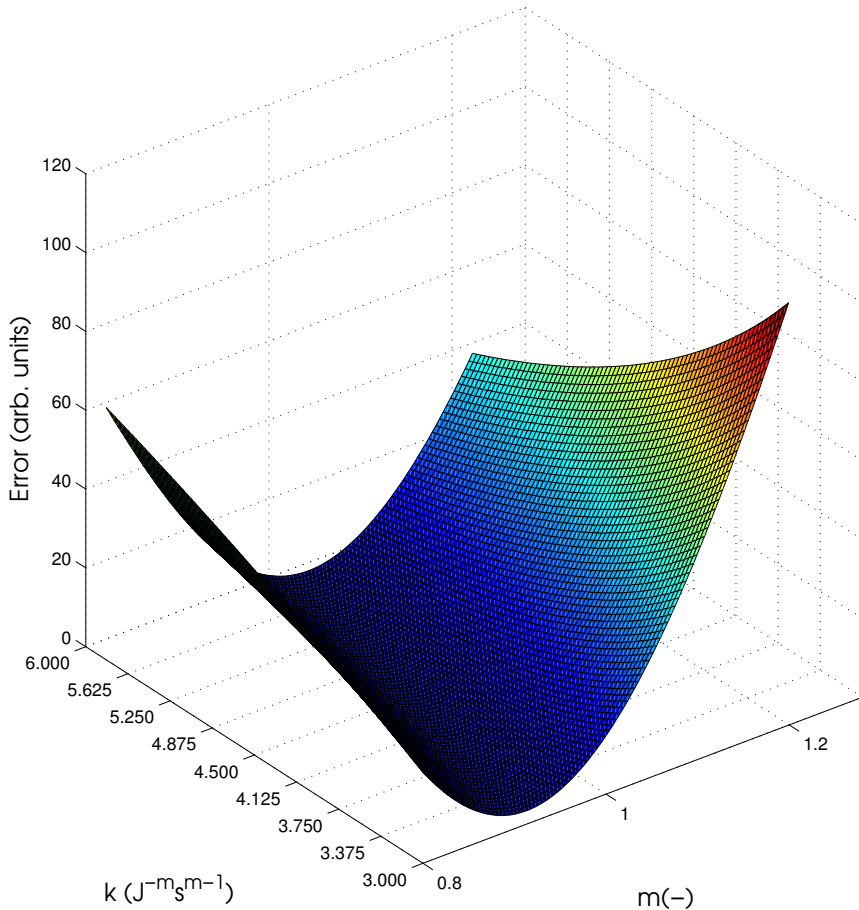


Figure 4.3: Surface plot of the absolute error of the bleaching model fit to the bleaching signal at 1mW laser intensity at 20.0 K. The error is minimized at $k = 4.36$ and $m = 0.97$.

From figure 4.4, we see the optimized fit reasonably coincides with the trace, although not perfectly. Since the minimized fit was very accurately determined by the high-resolution surface plot of figure 4.3, we suspect the process is not fully described by the model. The error is defined as the sum of squares of the distance between the fit and the data at every data point. The "minimal" error, if every of 4700 data points was 0.01 away from a perfect fit would be $4700 \times (0.01)^2 = 0.47$, where the best fit gave an error of 2.6.

However, for a lower laser intensities of 0.05 mW, the fit turned out to imprecise due to the k value, which shifts the graph up and down, but does not severely change the shape. The shape of the functional form is very alike that of the evidence of $m = 1$ is also strong for the lower intensity see figure 4.5. As observed, a smaller value of k would have minimized the fit error. The implication of the value of k being different for different intensities does not seem clear.

A problem for the higher laser intensity traces (figure 4.4) is that the signal does not decrease to zero in the time span measured, which could have caused the kink in these plot. Multiple processes could be causing a nonzero noise floor, as identified for higher powers in figure 4.2. One of these could be that lasers are also absorbed by other transitions present in the sample, causing the absorption not to head towards zero if all divacancies are bleached. Besides, it could be that the bleaching laser field is able to cause some repumping, causing continuous switching between two charge states and leading the signal not to decrease to zero, just as for particular laser frequencies in NV-centers.²¹ Next to these, materials specific effects, detector noise and reflections, causing transmission to be different from 1 despite no absorption by divacancies occurs, could all have caused the signal to be nonzero when the PL2 divacancies are fully bleached.

4.3.2 Fit of bleaching shapes to traces

Since the previous method did not fully confirm one of the possible values for m, we could also consider the bleaching process by emphasizing the shape of the signal curve under bleaching and comparing them to both

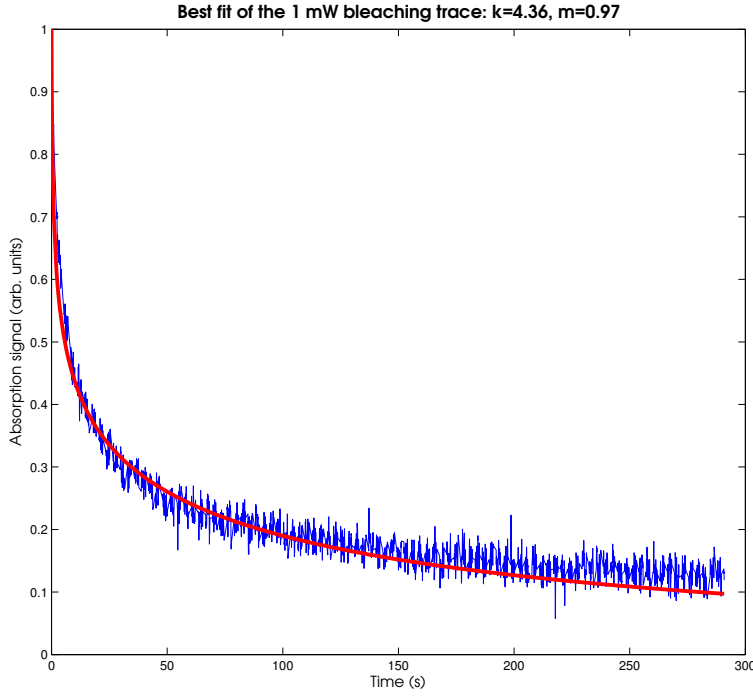


Figure 4.4: Plot of both trace and best model fit for $k = 4.36$ and $m = 0.97$ at 1 mW at 20.0 K.

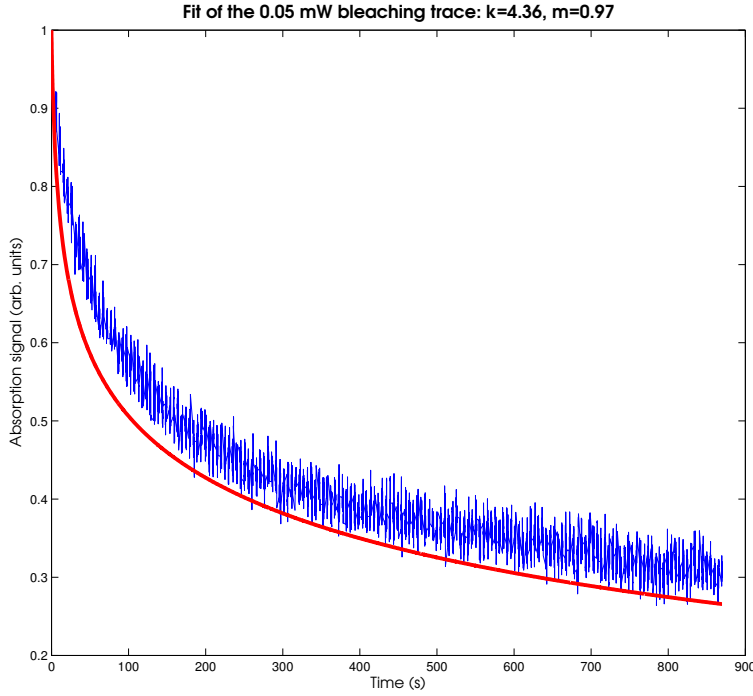


Figure 4.5: Plot of both trace and model fit for $k = 4.36$ and $m = 0.97$ at 0.05 mW at 20.0 K.

scenarios. Whether an ensemble is bleached by either a one- or two photon process influences the shape of the temporal trace. Figure 4.6 clearly shows the difference for $m = 1$ and $m = 2$ traces for both $100 \mu W$ and 1 mW for arbitrary k . For the lowest intensity, the $m = 1$ trace seems to fit the data much better than the $m = 2$ trace. For higher intensities, the result was slightly more ambiguous, as shown in figure 4.6b). The failure of $m = 1$ traces in favor of $m = 2$ traces to resemble the data at high intensities could be attributed to the signal to flatten out due to a nonzero noise floor (see section [5.3.1]) which favours $m = 2$ lines since these flatten out more than $m = 1$ lines.

Discussion

Considering the methods of both sections [5.3] and [5.4], the evidence is in favor of a single photon process. Hence, of the proposed process of figure 4.1 both single photon processes could be causing bleaching. Some of these gives rise to a positive charge state, whereas the other gives rise to the negative charge state. The repump process, which switches the charge state of the divacancies back to the initial charge state, should be a process opposite to the bleaching process: if -for example- an electron is extracted from the divacancy, the repump process should inject an electron into the divacancy. However, by only this method, it is not possible to determine whether a hole or an electron excitation is responsible for either bleaching or repumping.

Although repump traces were collected, the fact that repumping was performed with a pulsed laser made proper consideration difficult. The effective intensity for a short period is very high, but it is unknown how this intensity is exactly distributed over time and space. One could model such a laser field, but its characteristics need to be determined. One could also perform the same analysis as in section [5.3], but next to 'k' and 'm', 'I₀' still needs to be determined as well which makes it very unreliable to fit.

Also temperature showed to influence the bleaching effect. If the temperature is low (4.2 K) relative bleaching is really small, since linewidths are smaller and therefore the initial absorption is relatively low compared to the higher temperature case. By spin pumping, the electron population leaks away to levels having no resonant transitions with the applied laser field. At higher temperatures, the severe homogeneous broadening of excited state levels can cause a single laser to cause spin pumping, since excited state and ground state levels start to overlap. Therefore, bleaching was considered at a temperature of 20.0 K.

However, if the optical bleaching process can't be perfectly described by a single photon process, it could be that two processes, one depending on a single and one depending on multiple photon process are causing the charge state to change. This suspicion is raised by the observation that higher intensities show a kink in their bleaching trace.

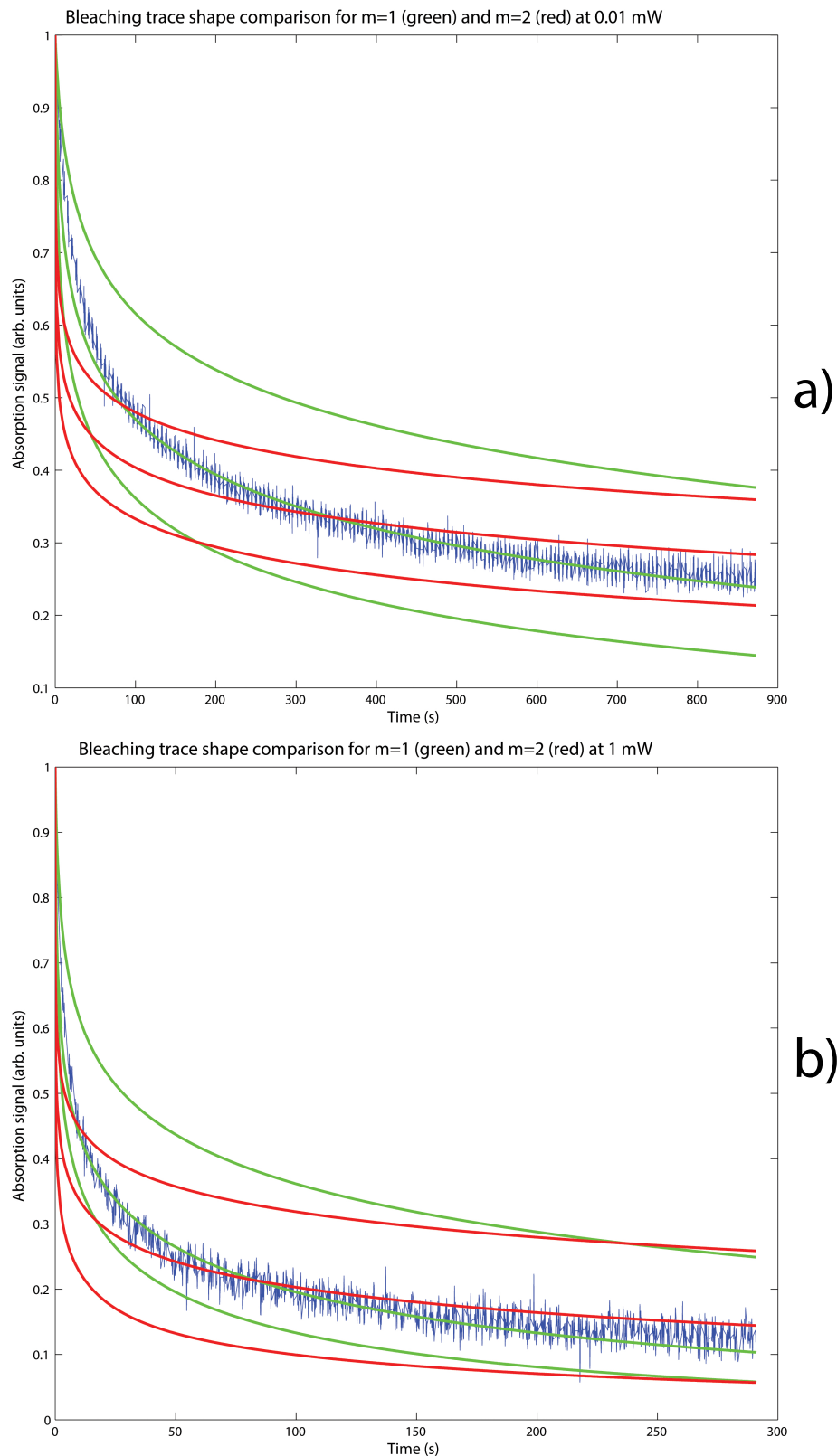


Figure 4.6: Actual bleaching traces (in blue) and three model traces for several k -values that show model traces close to the bleaching traces for $m = 1$ (green) and $m = 2$ (red) for both **a)** 0.1 mW **b)** 1 mW at 20.0 K .

5 Conclusion

5.1 Excited state structure

Using a lock-in technique to detect a magneto-spectroscopy scan, an attempt was made to unravel the excited state structure of the PL2 defect in Silicon Carbide. A model assuming a single triplet excited state, no forbidden transitions and no Inter System Crossing showed to be unable to explain all the features observed in a magneto-spectroscopy scan over two-laser detuning and magnetic field.

Two sets of defects have been distinguished: three features centered at 1130.50 nm and four lines centered at 1130.61 nm. It was found impossible to fit the two separate sets to two simple triplet-triplet models, which results to the conclusion that both different transition strengths and Inter System Crossing give rise to the two observed sets of magneto-spectroscopic features, if these originate from two triplet-triplet electronic structures.

An essential characteristic of these sets of features is that these probably originate from different physical defects, since bleaching a spectral hole in the features of one set did not show a spectral hole in the features belonging to the other carrier frequency. However, it can still be tested whether such an experiment does not lower the total level of the other carrier frequency's feature instead of a sharp dip.

Due to the observed interaction between features of both sets in figure 3.1, the hypothesis all magneto-spectroscopic features are originating from an excited state manifold is posed. Moreover, an interaction between two sets attributable to electronic population dynamics undermines the hypothesis of two independent defects with separate electronic structures. This also holds for the case of the third hypothesis of a non-continuous influence of strain on ISC and transition strength, since both electronic level structures belong to different physical defects. Methods able to test either of the three hypothesis have been reported in section [5]. These mainly rely on testing samples with different impurity concentrations, different divacancy concentrations and different strains. Different strains could as well be obtained by straining the sample intentionally or by using parts of the sample with a different local strain.

If either of these hypotheses is corroborated, by using a rate equation model, one can mimic the features observed by estimating the relevant splitting parameters to clarify the actual excited state structure of c-axis divacancies in SiC.

Coherent Population Trapping was observed in a spin pumping feature, where the 30 MHz wide CPT dip did not occur in the middle of the line. This observation led to the conclusion the magneto-spectroscopic feature consists of two spin pump features, which confirms the conclusion the simple spin pump model for triplet excited states does not hold.

5.2 Optical bleaching

We have observed persistent bleaching that altered the charge state of the PL2 divacancy causing spectral hole burning, being strongly dependent on incident laser power. Upon illumination, charge states were switched: resonant divacancies changed into non-resonant ones. It has also been observed that temperature alters bleaching: under lower temperatures, bleaching is a slower process due to smaller linewidths. By applying a 770 nm pulsed laser field, the absorption of the ZPL frequency was restored rapidly (in the order of seconds) by a sideband transition back to the old charge state.

Fitting a model mimicking the signal as expected by probabilistic intensity-dependent bleaching of the resonant charge state for a single ground and excited state led to the conclusion that it is very probable a single photon process causes optical bleaching in PL2 divacancies in Silicon Carbide. The bleaching effect is therefore one of the three single excitations of figure 4.1. However, the analysis section [5.3] is not able to determine whether bleaching is a hole or an electron excitation and hence not able to determine whether the bleached charge state is a positive or negative one.

Imperfections of the bleaching traces have been identified: random noise and processes as absorption by other defects and slight repumping at the applied laser frequency could have caused the bleaching not to behave as in the ideal case, causing the fit of section [5.3.1] not to be perfect.

It was found that the repump process was much faster than the bleaching process: the 125 μW trace of repumping had a similar reverse effect than the 3500 μW bleaching trace after a particular time. No attempt was made to fit the repump to a functional form as done for bleaching, since the used laser was a pulsed wave laser and no functional model was fitted with the data since the effective intensity was unknown. However, using a continuous wave laser, one could perform a similar analysis as for bleaching. Additionally, the electronic structure in the charge state when bleached is not known. Therefore, it is hard to specify processes underlying the repumping process.

An experimental improvement that could have been made is by only considering divacancies in a sample

illuminated with a single laser intensity. Although the method in section [5.2] took the spatial intensity distribution into account, an inhomogeneous laser intensity could have altered the appropriateness of the fitting method due to a slightly non-ideal Gaussian laser spot. A signal from only homogeneously illuminated divacancies can be obtained by placing apertures much smaller than the FWHM behind the sample. However, using small apertures diffraction effects could complicate photon collection.

5.3 Conclusion

In this thesis, we gave an overview of current research in quantum information research concerning spin manipulation schemes in Λ systems in divacancies in SiC. Next to that, a setup able to show spin manipulation, spectroscopic features and bleaching by PLE and in transmission techniques was discussed.

Assuming the electronic structure can be considered as a simple structure as shown in figure 4.1, strong evidence was posed for a one-photon bleaching process. By using a continuous wave laser for the repump process, it can be investigated similar to the bleaching process to investigate whether it is a single or a two photon process. The excited state structure of PL2 defects is still not well understood. The defects showed two sets of magneto-spectroscopic features possibly not belonging to the same physical defects. If a bleaching experiment shows no relation to the two sets, these could attributed to either two sets of different defects close in resonance frequency or a discontinuous effect of strain leading to two sets of defects resembling other D and E parameters and different selection rules and ISC strengths. These hypotheses can be tested by straining the sample and by different divacancy and impurity concentrations.

An important consideration for qubit systems is increasing the effective coherence time of the material, T_2^* , for more reliable quantum communication and computation schemes. By decreasing the influence from spin-spin and nuclear spin fluctuations by using homogeneously strained divacancies and nuclear polarizations, the electron spin its decoherence time could be increased. This is essential to practical applications, since long coherence times allow for optical manipulation by initializing quantum states and reading out for computation.

Another important branch of future research aims at communicating with a homogeneous ensemble in order to increase coherence times and to have more fidelity in photon-electron spin communication. To reduce inhomogeneous broadening issues for optical spin manipulation, one could bleach a part of the inhomogeneously broadened ensembles to another charge state, to arrive at a narrower, less-broadened ensemble of divacancies. This allows to prepare a better controlled quantum state where the defects present can be used in an optimal way. However, the spectral width of bleaching proved to be much wider (10 MHz) than the laser (see section [3.1]) bandwidth which complicates selective bleaching. Next to this, downscaling the size of a single qubit system smaller than a large ensemble of defects is of importance to reach the objective of making a quantum computing system competitive to classical computers.

References

- ¹ Kimble, H. J. The quantum internet. *Nature* **453**, 1023 (2008).
- ² Ekert, A. K. Quantum cryptography based on bell's theorem. *Physical Review Letters* **67**, 661 (1991).
- ³ Bennett, C. H. & Brassard, G. Quantum cryptography: Public key distribution and coin tossing. In *Proceedings of the IEEE International Conference on Computers, Systems and Signal Processing* 175 (1984).
- ⁴ Casady, J. B. & Johnson, R. W. Status of silicon carbide (sic) as a wide-bandgap semiconductor for high-temperature applications: A review. *Solid-State Electronics* **39**, 1409 (1996).
- ⁵ Koehl, W. F., Buckley, B. B., Heremans, F. J. & Calusine, A. D., G. Room temperature coherent control of defect spin qubits in silicon carbide. *Nature* **479**, 84 (2011).
- ⁶ Falk, A. L. *et al.* optical polarization of nuclear spins in silicon carbide. *Physical Review Letters* **114**, 247603 (2015).
- ⁷ Zwier, O. V., O'Shea, D., Onur, A. R. & van der Wal, C. H. All-optical coherent population trapping with defect spin ensembles in silicon carbide. *Scientific Reports* **5**, 10931 (2015).
- ⁸ Fleishhauer, M., Imamoglu, A. & Marangos, J. P. Electromagnetically induced transparency: optics in coherent media. *Review of modern physics* **77**, 633 (2005).
- ⁹ Griffiths, D. J. *Introduction to Quantum Mechanics* (Pearson, 2014), 2nd edn.
- ¹⁰ Cohen-Tannoudji, C., Diu, B. & Laloe, P. *Quantum Mechanics* (Wiley, 1977), 1st edn.
- ¹¹ Christle, D. J. *et al.* isolated electron spins in silicon carbide with millisecond coherence times. *Nature Materials* **14**, 160 (2015).
- ¹² Hanson, R. & Awschalom, D. D. Coherent manipulation of single spins in semiconductors. *Nature* **453**, 1043 (2008).
- ¹³ Maze, J. R. *et al.* properties of nitrogen-vacancy centers in diamond: group theoretic approach. preprint at: <http://arXiv.org/abs/1010.1338v1> .
- ¹⁴ Santori, C. *et al.* coherent population trapping in diamond n-v centers at zero magnetic field. *Optics Express* **14**, 7986 (2006).
- ¹⁵ Jobez, P *et al.* Coherent spin control at the quantum level in an ensemble-based optical memory. *Physical Review Letters* **114**, 230502 (2015).
- ¹⁶ Heinze, G., Hubrich, C. & Halfmann, T. Stopped light and image storage by electromagnetically induced transparency up to the regime of one minute. *Physical Review Letters* **111**, 033601 (2013).
- ¹⁷ Turukhin, A. V., Sudarshanam, V. S. & Shahriar, M. S. Observation of ultraslow and stored light pulses in a solid. *Physical Review Letters* **88**, 023602 (2002).
- ¹⁸ Fu, K.-M. *et al.* Observation of the dynamic jahn-teller effect in the excited states of nitrogen-vacancy centers in diamond. *Physical Review Letters* **103**, 256404 (2009).
- ¹⁹ Fox, M. *Optical Properties of Solids* (Oxford University Press, 2010), 2nd edn.
- ²⁰ Moerner, W. *Persistent Spectral Hole-Burning: Science and Applications* (Springer, 1988), 1st edn.
- ²¹ Beha, K., Batalov, N. B., A Manson & Bratschitsch, A., R Leitenstorfer. Optimum photoluminescence excitation and recharging cycle of single nitrogen-vacancy centers in ultrapure diamond. *Physical Review Letters* **109**, 097404 (2012).
- ²² Oppenheim, A. V., Willsky, A. S. & Young, I. T. *Signals and systems* (Prentice-Hall, 1983), 1st edn.

A Frequency Spectra of IDQ ID230 Photon Counter Signal

In order to optimize the Signal to Noise-Ratio (SNR) of a measurement device, it is useful to determine the frequency spectrum of the total signal when illuminated and the noise spectrum only. Here, such frequency spectra of a Single Photon Counter (SPC), an IDQ ID230 were determined. After the determination of the noise its frequency origin, one could filter the frequency spectrum to minimize noise and to increase the SNR. Using Fourier analysis one finds:²²

$$X(\omega) = \frac{1}{T} \int_{-\infty}^{\infty} x(\tau) e^{-i\omega\tau} d\tau \quad (10)$$

Where $x(\tau)$ is the time trace of the photon counter. One can find the power spectral density, a more frequently used method to determine noise spectra, to determine in which frequencies the power of the signal is concentrated. The power spectral density is found by Parseval's identity:

$$\int_{-\infty}^{\infty} |x(t)|^2 dt = \frac{1}{2\pi} \int_{-\infty}^{\infty} |X(\omega)|^2 d\omega \quad (11)$$

Hence, the square of the frequency component coefficient of a fourier series is the power density in that particular frequency. The power spectral density was computed using a sum approximation of the fourier integral of the signal and noise spectra were taken for three different conditions:

- Severe laser illumination: 10 mW before the sample with factor $9 * 10^6$ neutral density filters in front of a coupling fiber
- Moderate laser Illumination: 10 mW before the sample with factor $3 * 10^7$ neutral density filters in front of a coupling fiber
- No laser illumination, only background light

The light was collected in a coupling fiber that directed the light towards the photon counter. A time trace that gave pulses when a certain buffer of counts was reached was processed to a signal trace with even periods. The minimal frequency one can distinguish with a trace of a time T is given by $1/T$. The maximum frequency one can distinguish is given by $1/(2\Delta T)$, where ΔT is the sampling time. Hence, the non-illuminated trace has a lower maximal frequency, since there were less time bins, since it took longer before the buffer was reached. A fourier transform of this signal trace was performed and a power spectral density was computed. In figure A.1, one observes that the power density is gradually decreasing with frequency for all three cases. Hence, the noise is not concentrated in a particular frequency range and hence, blocking particular frequencies does not improve the SNR of the system.

B Hamiltonian of a Triplet Orbital State

The spin state Hamiltonian of the neutral divacancy is given by:

$$H_{g,e} = D_{g,e} \sigma_z^2 - E_{g,e} (\sigma_x^2 - \sigma_z^2) + g \mu_0 \vec{B} \cdot \vec{S} \quad (12)$$

Here, $D_{g,e}$ denotes the crystal field splitting from spin-spin interactions and $E_{g,e}$ denotes the crystal field splitting due to the anisotropy of the crystal. g refers to the Landé factor for electrons. The last term denotes the Zeeman splitting due to an applied magnetic field. The perturbation to the Hamiltonian in the rotating frame by applying two laser fields is given by equation (13).⁸ Ω_p and Ω_c are the Rabi frequencies of the probe laser and the coupling laser, respectively. Δ_1 denotes the detuning between the probe laser and the transition between the first and the third level and Δ_2 denotes the detuning between the control laser and the second and third level.

$$H = \begin{pmatrix} 0 & 0 & \Omega_p \\ 0 & -2(\Delta_1 - \Delta_2) & \Omega_c \\ \Omega_p & \Omega_c & -2\Delta_1 \end{pmatrix} \quad (13)$$

By altering the probe and control Rabi frequencies over time, it is possible to prepare the system in a particular dressed state, in which the system is in a specific dark state.⁸ An example of such a dark state is given in section [1.2].

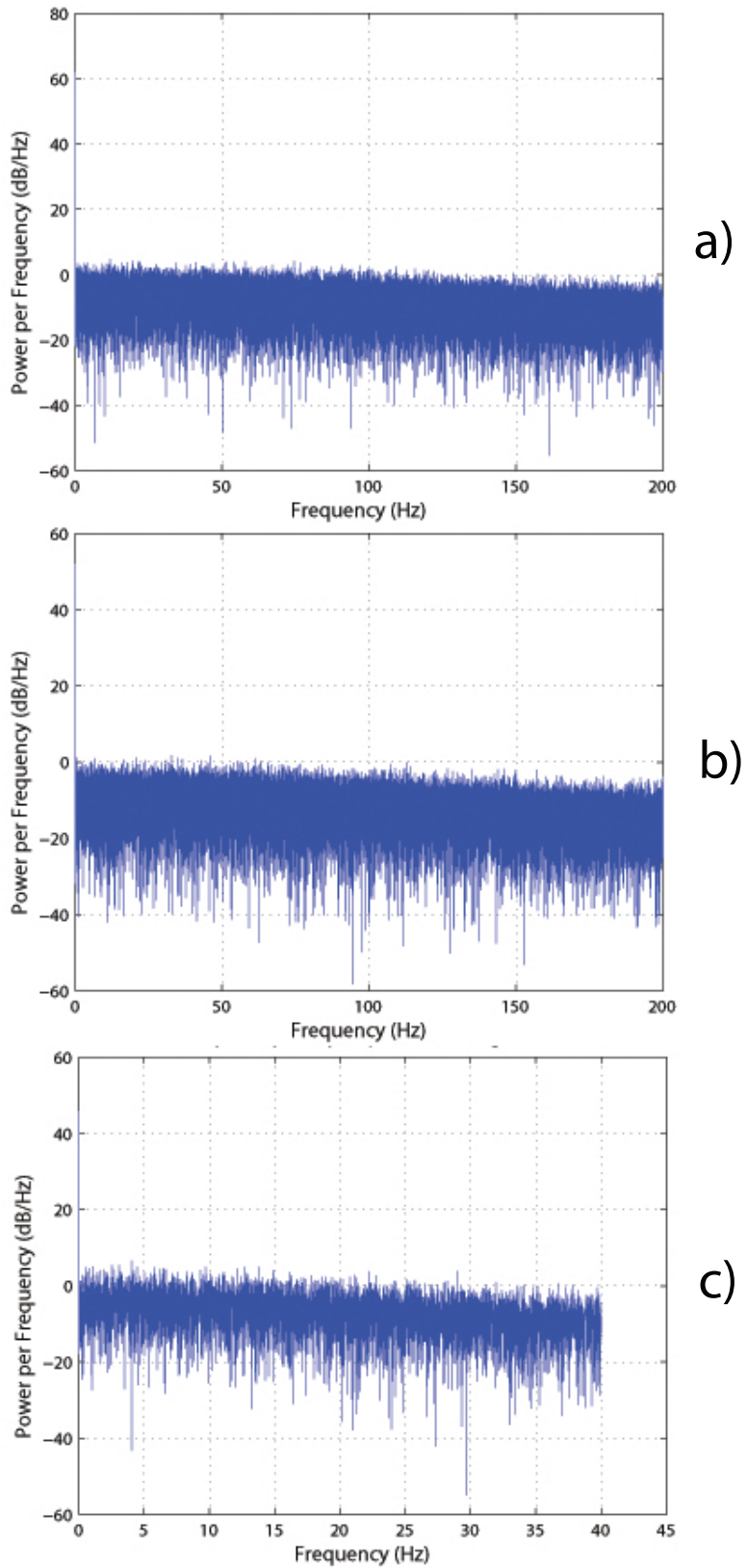


Figure A.1: Power spectral densities for **a)** severe illumination, close to photon counter saturation **b)** moderate illumination **c)** no laser illumination of the IDQ ID230 Single Photon Counter. The traces are normalized to power density of the first frequency.